Title: AN OPEN-SOURCE DEVELOPMENT BASED ON PHOTOGRAMMETRY FOR A REAL-TIME IORT TREATMENT PLANNING SYSTEM

Authors:

[1]*Sergio Lozares-Cordero, [2]Carlos Bermejo-Barbanoj, ,[3]Alberto Badías-Herbera, [4]Reyes Ibáñez-Carreras, [5]Luis Ligorred-Padilla, [4]José Miguel Ponce-Ortega, [6]Víctor González-Pérez [1]Almudena Gandía-Martínez, [1]José Antonio Font-Gómez, [7]Olga Blas Borroy [2]David González-Ibáñez

Affiliations:

1: Physics and Radiation Protection Department- Miguel Servet University Hospital (Zaragoza-Spain).

2: Aragon Institute of Engineering Research- University of Zaragoza (Spain).

3: Higher Technical School of Industrial Engineering- Polytechnic University of Madrid (Spain).

4: Radiation Oncology Department- Miguel Servet University Hospital (Zaragoza-Spain).

5: Esophagogastric Surgery and Sarcoma Unit (Department of General and Gastrointestinal Surgery) – Miguel Servet University Hospital (Zaragoza-Spain).

6: Medical Physicist Department- IVO Foundation (Valencia- Spain).

7: Engineering and Maintenance Service– Miguel Servet University Hospital (Zaragoza-Spain).

Corresponding author: *Sergio Lozares-Cordero

slozares@salud.aragon.es

sergiolozares@gmail.com

Institution: Miguel Servet University Hospital (Zaragoza-Spain).

Contact information for the corresponding author:

Phone: (+34) 605 743113

Paseo Isabel la Católica 1-3

50009 Zaragoza (Spain)

NO CONFLICT OF INTEREST

HIGHLIGHTS

- A TPS for low-energy photon IORT based on photogrammetry was developed.
- The 3D images are reconstructed from a video obtained with a smartphone or tablet.
- Absorbed doses are calculated with the TG-43 algorithm on the reconstructed images.
- All carried out live, inside the operating room, in real time.
- Commissioning was carried out with radiochromic films.

ABSTRACT

Purpose: This study presents a treatment planning system for intraoperative low-energy photon radiotherapy based on photogrammetry from real images of the surgical site taken in the operating room.

Material and methods: The study population comprised 15 patients with soft-tissue sarcoma. The system obtains the images of the area to be irradiated with a smartphone or tablet, so that the absorbed doses in the tissue can be calculated from the reconstruction without the need for computed tomography.

The system was commissioned using 3D printing of the reconstructions of the tumor beds. The absorbed doses at various points were verified using radiochromic films that were suitably calibrated for the corresponding energy and beam quality.

Results: The average reconstruction time of the 3D model from the video sequence in the 15 patients was 229,6 ± 7,0 s. The entire procedure, including video capture, reconstruction, planning, and dose calculation was 520,6 ± 39,9 s. Absorbed doses were measured on the 3D printed model with radiochromic film, the differences between these measurements and those calculated by the treatment planning system were 1.4% at the applicator surface, 2.6% at 1 cm, 3.9% at 2 cm and 6.2% at 3 cm.

Conclusions: The study shows a photogrammetry-based low-energy photon IORT planning system, capable of obtaining real-time images inside the operating room, immediately after removal of the tumor and immediately before irradiation. The system was commissioned with radiochromic films measurements in 3D-printed model.

Keywords: IORT, TPS, photogrammetry, radiochromic films, electronic brachytherapy

INTRODUCTION

Intraoperative radiation therapy (IORT) involves the administration of radiation during surgery. However, the high single dose poses a potential risk of increased late toxicity if not appropriately delivered.

Soft tissue sarcomas (STS) are a rare and heterogeneous group of malignant diseases [1]. Modern oncology not only emphasizes tumor control and survival but also preservation of functioning and quality of life [2,3]. Therefore, less invasive surgery with smaller margins can be combined with additional local treatment modalities such as IORT, to maintain adequate local control while achieving better functional outcomes and quality of life [4].

The use of intraoperative volumetric real-time imaging to evaluate applicator placement and optimize the treatment plan is only feasible if an imaging device that can calculate density relative to water, such as computed tomography (CT), O-arm cone beam CT (CBCT), and C-arms CBCT [5,6], is available in the operating room (OR) [7,8]. Other systems are under development to enhance the accuracy of the dose administered in IORT treatments [9].

This study employs a photogrammetry-based approach to generate images and optimize tumor treatment. The images are obtained using a smartphone or tablet and subsequently processed. Photogrammetry involves measuring an object through images—photographs or a video sequence—captured using a camera. The captured image is the projection on a two-dimensional (2D) plane of a three-dimensional (3D) scene, in which the information relating to depth is lost [10]. Photogrammetry also allows the reverse process, i.e., obtaining the 3D scene from multiple photographs of the same scene. One of the most common techniques is to compare images, looking for characteristic points of the scene in each of them. Once the characteristic points are defined, a cloud of points is obtained. This is then densified, yielding a 3D mesh that represents the scene [11].

Once the 3D image of the tumor bed is obtained, the absorbed dose is calculated on the object's surface using the TG-43 formalism [12,13], resulting in a simple treatment planning system (TPS) for IORT.

The objective of this study is to develop a simple TPS to be used in the OR to evaluate the absorbed doses in an IORT treatment with 3D images reconstructed (based on photogrammetry) from a video sequence captured with a smartphone or tablet.

Subsequently, the TPS will be commissioned by printing the tumor bed obtained in 3D and measuring the absorbed dose at different points using suitably calibrated radiochromic film.

MATERIALS AND METHODS

Patients:

Our study included a cohort of patients who were selected by the surgical team and evaluated by the multidisciplinary sarcoma committee at our hospital. All patients provided informed consent that was approved by the ethics committee of the Aragonese Health Service. All methods were conducted in compliance with applicable guidelines and regulations.

The cohort consisted of 15 patients (9 men and 6 women) aged 17-77 years (mean age, 57 years) with tumors in various locations (mainly retroperitoneal) who were treated between May 2019 and December 2022. All tumors were soft tissue sarcomas (9 liposarcomas, 6 leiomyosarcomas). The prescribed dose was 20 Gy at the surface of the applicator in contact with the tumor bed, with a median fill volume of 60 cc. Pre-planning was performed in all cases using available imaging sets (MRI, CT, or PET-CT). The main organs at risk (OAR) were the abdominal organs and large blood vessels in the treatment area.

IORT was administered using the Xoft Axxent® electronic brachytherapy system (Xoft, Inc., a subsidiary of iCAD, San Jose, CA, USA), which is a high-dose-rate brachytherapy method based on a balloon applicator and an electronic brachytherapy source. The source is a vacuum tube (10 mm in length, 2 mm in diameter) enclosed in a cooling catheter (5.6 mm diameter). It operates at 50 kVp with 300 µA of electrons striking a thin tungsten film target on the inner surface of a ceramic X-ray-transparent anode [14].

Three-dimensional imaging

In our study, we employed photogrammetry, which utilizes a camera to capture images and allows for video sequences to be analyzed. We utilized AliceVision Meshroom [15], a freely available 3D reconstruction software application, to perform volumetric reconstruction with photogrammetry. To do so, we utilized an Android smartphone camera (Bq Aquaris X) and a tablet (NVIDIA SHIELD tablet K1), which were appropriately calibrated using Matlab software [16]. The calibration was necessary to determine lens distortion and the intrinsic parameters of the camera used, which included focal length in the X and Y directions, center, radial distortion, tangential distortion, and the optical center of the image sensor [17].

The video recording process did not require specific conditions, but we recommend using a high resolution, such as FullHD (1920 x 1080 pixels) resolution, and standard frame rates within the range of 30-60 fps to ensure enough frames. Photogrammetry enables the reconstruction of a scene or an object in 3D using 2D images. This technique recovers the depth information from multiple images of the scene, as images are compared to obtain common points. Subsequently, a point cloud is generated, and depth maps are estimated.

To achieve a quality model, the 3D reconstruction process involves the use of depth maps and CUDA libraries for fast reconstruction of the scene. Consequently, hardware with an NVIDIA GPU graphics card is necessary for faster post-processing, although slower techniques such as Draft Meshing can be used without the card to enable a dense reconstruction of the model. The model's textures are obtained and can be superimposed on the mesh obtained (Fig 1).

Simulation of Dose Distribution

Following the 3D reconstruction, simulation of the applicator placement is conducted in the planning software. A prescribed dose is then assigned to the surface of the applicator, with a prescription of 20 Gy at the applicator surface chosen based on existing literature for the 15 patients treated. The software is used for verification, and the main organs at risk (OARs) in retroperitoneal STS are identified as the colon, duodenum, intestine, and stomach [18].

The absorbed dose distribution is reproduced in real-time using the software developed, following computation of the 3D model. The points at which the dose is absorbed are evaluated at different distances to represent the OARs in each case study. The absorbed dose distribution is calculated using the TG-43 formalism [12,13], which involves a set of mathematical equations that describe the radiation dose rate around a point source in a homogeneous medium. The TG-43 formalism considers various physical and dosimetric parameters, including the source strength, the distance between the source and the point of interest, and the attenuation and scatter of the radiation in the medium.

In the case of the Axxent system, the TG-43 formalism is used to calculate the dose distribution in the tissue surrounding the applicator. This information is utilized to optimize the treatment plan and ensure that the desired dose is delivered to the target while minimizing the absorbed dose to surrounding healthy tissue. This approach is widely used in brachytherapy and IORT procedures.

The computational model is implemented in Matlab (The Mathworks, Inc. MA, USA) and subsequently in OpenGL to develop a fast tool to estimate dosimetry and determine how treatment parameters are affected in real-time.

An optimized code is implemented in Matlab v.9.6 R2019a to speed up the computation, allowing complex 3D geometries to be run, with the format used for the 3D model files being "*.PLY".

For every vertex of the model, the absorbed dose is obtained using the "TG-43_fun" function, which implements the TG-43 formalism equations used to estimate the absorbed dose for a single point. The dwell positions, dwell times, and source-related parameters are defined, and the absorbed dose is calculated. The dose rate is calculated for every dwell position (Equation 1), and the contribution of each dwell position to the total dose is calculated as the product of the dose rate and the dwell

time (Equation 2). Finally, the total absorbed dose is calculated as the sum of all the contributions from each dwell position (Equation 3).

To increase the computation speed and reduce resource consumption, the function is vectorized, allowing almost real-time results to be obtained. The 3D model is displayed as a point cloud, where every point has its absorbed dose value associated. The 3D visualization facilitates the interpretation of the results for the dose distribution.

$$\dot{D}(r,\theta) = S_K \cdot \Lambda \cdot \frac{G_L(r,\theta)}{G_L(r_0,\theta_0)} \cdot g_L(r) \cdot F(r,\theta) \quad (1)$$

$$D(r,\theta) = \dot{D}(r,\theta) \cdot \frac{Time(s)}{3600} \quad (2)$$

$$D_{P,Total} = \sum_{i=1}^{N} D_{P,i} \quad (3)$$

Where Sk is the air kerma strength of the source, Λ is the dose-rate constant, G(r, θ) is the geometry factor, F(r, θ) is the anisotropy function, r denotes the distance (in centimetres) from the center of the active source to the point of interest, r_0 denotes the reference distance which is specified to be 1 cm in this protocol, and θ denotes the polar angle specifying the point-of interest, P(r, θ), relative to the source longitudinal axis. The reference angle, θ_0, defines the source transverse plane, and is specified to be 90° or π/2 radians (Fig. 2). Equation 2 illustrates the dose rate contribution emanating from a particular dwell position, which is then multiplied by the corresponding dwell time. Lastly, Equation 3 demonstrates the contribution of each dwell position towards the absorbed dose at point P.

Code Implementation in C++ and OpenGL

Due to the limitations of the MATLAB representation of 3D models, which cannot handle real-time movement and representation of the entire model at the necessary rates, we decided to migrate the code to C++ and use OpenGL to calculate and represent the dose with no loss of time. The primary objective was to increase the refresh rate in the representation, thereby achieving real-time results without relying on MATLAB's licensed software. We constantly calculate the absorbed dose using OpenGL whenever the applicator rotates, or a parameter changes. To accomplish this, we use "shaders[1]" that update the display every time there is a change. The shaders run on the GPU of the device, allowing the code to run simultaneously on each of its processors. The shaders are written in GLSL v4.1, the OpenGL Shading Language.

[1] User-defined program designed to run on GPU. Shaders preform graphical calculations, are written in their own programming language (Shading Languages, for instance GLSL) and are compiled separately from the main program.

We added a user-friendly graphical interface [19] that enables the user to modify the processing data with the CVUI [20] library implemented in OpenCV. The shader inputs are defined in the main function (uniforms[2]) for the TG-43 formalism, including the dwell position, dwell time, effective source length, Reference Air Kerma Rate (RKRA), dose rate constant (Λ), and maximum rendering scale value. Eight dwell positions were defined since this number is not exceeded in the clinical cases analyzed. A "trackbar" was defined for each of the modifiable parameters in the user interface, and a color scale was included to aid interpretation.

Once the application is launched, the geometry is loaded, and the vertex information is extracted. The default parameters defined for the application (reference parameters for one of the studied clinical cases) are loaded. Two windows are opened: a viewport, where the geometry with the absorbed dose superimposed is shown, and a GUI (Graphical User Interface), which allows the user to modify the parameters previously defined.

The absorbed dose is calculated using a shader while the viewport remains open. This shader implements the TG-43 equations (Equations 1 – 3), which are also implemented in the MATLAB prototype, and applies them to all the vertices at once, utilizing GPU optimization for parallel computation. Whenever the user changes the point of view or a treatment parameter, the shader updates the information and recalculates the dose for every vertex of the model. With the power of today's General Purpose GPU (GPGPU), this calculation can be done in real-time, even for large models with hundreds of thousands of vertices. The code is available in an open-source repository: http://github.com/cberbarbanoj/TG-43-Estimator.

Absorbed dose verification

Measurements of absorbed dose were carried out using plastic water slabs (PWDT: CIRS, Norfolk, VA) [21] to verify the dose measurements at different depths. Based on these measurements, a percentage depth dose (PDD) was constructed and compared with the PDD provided by the manufacturer, which was measured with an ExRadin A20 ionization chamber (Standard Imaging Inc.), a TM23342 ionization chamber (PTW, Freiburg, Germany), and radiochromic films using all applicators (Fig 3).

Furthermore, the absorbed dose in water was measured using radiochromic films in a mini water phantom (Fig 4). This allowed for verification of absorbed dose at known distances in a homogeneous medium at the surface of the applicator surrounded by water.

[2] Global shader variable, declared with the “uniform” storage qualifier. Uniforms are defined in the main code of the software and can be accessed by all the shaders of the program. Uniform values remain constant until they are reset or updated to another value, either by an instruction in the function code itself or by user command. It is one of the ways in which information can be passed from an application, running on CPU, to a shader, running on GPU.

To verify the absorbed dose provided by the TPS and commission the software, radiochromic films were used and 3D-printed models were created from photogrammetric images of 15 patients. The model was 3D-printed using a Form 3B+ printer (Formlabs Inc., MA, USA) [22] with an Elastic A50® [23] material, "medical" type, having similar density to tissue. The printing was performed with SLA technology and an XY resolution of 25 µm and a layer thickness of 100 µm (Fig 5). A 5x5x5 cm^3 block of Elastic A50® was constructed, which was then scanned using a Brilliance CT scanner (Phillips Inc.) to determine its electron density. The average electron density was found to be 1.01±0.1 g/cm^3.

Once the model was created, clinically relevant points were identified, and the absorbed doses were calculated at these points by the TPS (Fig 6). The system was commissioned by re-delivering the patient's treatments on the 3D-printed phantoms and placing suitably calibrated small pieces of radiochromic film at each of these points to determine the differences between the absorbed dose measured and the absorbed dose calculated by the TPS (Fig 7).

Calibration of Radiochromic Films

Radiochromic film is commonly used as a detector for in vivo dosimetry verification [24–26], and various types of commercially available radiochromic films differ in their optimal response energy range and absorbed dose [27]. In this study, XR-RV3 radiochromic film was used to measure absorbed doses, which is specific for energies greater than 20 kVp and absorbed doses up to 30 Gy [28].

The radiochromic film used for measurement must be calibrated appropriately using a calibration method that has been previously used with the same film model and irradiation source [29,30]. The absolute dose evaluations of the irradiated films were obtained following established protocols for GafchromicTM XR-RV3 films [28,31].

The multichannel method with the Multigaussian approach calibration algorithm was used in this study. This method considers that the probability of the response vector z (i.e., the vector with the responses z_k for each channel) follows a multivariate Gaussian distribution, given a dose D [29]. The information from the three reading channels (red, green, and blue) was weighted differently based on the covariance matrix.

$$P((z|D) \sim N_k\big(\mu(D), \Sigma(D)\big) \qquad (4)$$

where, k is the number of different channels (i.e., irradiated channels and optionally nonirradiated channels), µ is the vector of expected values of the response and ∑ is the covariance matrix.

$$\Sigma_{ij} = cov\big[z_i, z_j\big] = E[(z_i - \mu_i)(z_j - \mu_j) \qquad (5)$$

The absorbed dose values were obtained for 0-25 Gy in 12 steps, and the measurements were read and processed using the Radiochromic.com v3.0 software application (Radiochromic SL, Benifaió, Spain) to calculate the calibration function.

Model XR-RV3 (batch 02141901) films were custom-calibrated by cutting pieces of film measuring 5 × 5 cm^2 and were marked and numbered to maintain their orientation in an Epson Expression 12000 XL scanner.

The films were scanned before and after irradiation, with post-irradiation scanning performed 24 h later. The scanner was warmed up 1 h before use, five scans were made before the films were scanned to warm up the light source, both before and after irradiation. The films were scanned (RGB 48-bit) in portrait orientation, one by one, with a resolution of 75 dpi using Epson Scan software and reflection mode.

The maximum optical density range was applied, and all the image corrections and filters were switched off. No correction was applied to address heterogeneity in the scanner response, since in no case was there an area greater than 6 × 6 cm^2 in the central part of the scanner. Here, uniformity was 0.3%, following the method used by Richter et al [32]. Each film was scanned consecutively 5 times and saved as a TIFF file.

The calibration curve was calculated by selecting a region of interest of 1 × 1 cm^2 to which the dose value previously measured using the ionization chamber was assigned.

Dose measurement uncertainties with radiochromic films were estimated (Table 1) to be 10.4%[28,31,33].

Table 1:Uncertainty analysis for measured film data expressed as a percentage.

Determination of dose at other points in water			**Uncertainty (%)**	
N_K from calibration laboratory			1.0	Calibration Certificate
Effect of beam-quality difference between calibration and measurement			2.0	TG-61[34]
Backscatter factor B_w			1.5	TG-61[34]
$P_{stem,air}$			1.0	TG-61[34]
$\left[\left(\frac{\bar{\mu}_{en}}{\rho}\right)^{w}_{air}\right]_{air}$			1.5	TG-61[34]
In-air measurement in the user`s beam			1.5	TG-61[34]
Combined standard uncertainty for $D_{w,z=0}$			**3.6**	
Determination of dose at other points in water			3.0	TG-61[34]
Combined standard uncertainty for $D_{w,z}$			**4.7**	
Uncertainty parameter	**Type A**		**Type B**	
Determination of dose at other points in water			4.7	
Beam uniformity			0.3	McCabe et al[28]
Film-to-film uniformity in 1 batch			1.0	McCabe et al[28]
Dose-rate film response			1.5	McCabe et al[28]

Setup error and film positioning			0.3	McCabe et al[28]
Multichannel algorithm uncertainty			1.0	Vera-Sánchez et al[33]
Shutter error			0.1	McCabe et al[28]
Pixel value uncertainty within ROI	0.8			
Scan-to-scan uncertainty	0.1			
Sterilization process	0.5			
Scanner drift	0.1			
Quadratic sum	1.0		5.1	
A and B quadratic sum		5.2		
Dose per film response % uncertainty (k=1)		5.2		
Dose per film response expanded % uncertainty (k=2)		±10.4		

Depth doses in water were obtained from absorbed dose measurements at the surface and by applying the TG-61 protocol [34]. PDD data were obtained from the manufacturer based on measurements averaged over 10 sources with different applicators, and these results were verified by measuring with the TM23342 ionization chamber and plastic water slabs (PWDT: CIRS, Norfolk, VA) based on the protocol for the TRS-398 formalism [35]. The results obtained were similar.

RESULTS

The PDD curve obtained from the TM23342 ionization chamber, the curve calculated from the manufacturer data, and the measurement taken with XR-RV3 exhibited good agreement (Fig 8).

Measurements of absorbed dose on the surface of the applicator, in the mini water tank, produced results equivalent to those obtained on the surface of the applicator measured in the 3D model, with differences of only 1.3% (1%-2%).

The measurements were repeated with different applicators to establish calibration curves for the radiochromic films. Five different calibration curves were constructed using various applicators to improve the accuracy of the results (Fig 9). The optical density (OD) was calculated using Eq. (1) [36,37]:

$$netOD = OD_{exp} - OD_{unexp} = \log_{10} \frac{PV_{unexp} - PV_{bckg}}{PV_{exp} - PV_{bckg}} \quad (6)$$

where PV_{unexp} and PV_{exp} are the readings for unexposed and exposed film pieces for each film, respectively, and PV_{bckg} is the zero-light transmitted intensity value.

The tumor beds were reconstructed using photogrammetry techniques, which provided 3D scenarios for verifying the absorbed doses. The total mean time for treatment planning was approximately 522.6 ± 45.7 s (465 s – 591 s), of which 227.8 ± 7.1 s (216 s – 239 s) was necessary for reconstructing the 3D model scenario (Table 2). The time required to capture the video scene to create the computational model was 30.3 ± 1.3s (28 s–32 s).

Table 2:Times for the different parts of the procedure and total time. (SD: standard deviation)

Patients	Video capture (s)	3D model (s)	Planning (s)	Total (s)
1	32	228	280	540
2	29	220	290	539
3	30	221	340	591
4	29	225	230	484
5	31	229	240	500
6	30	216	312	558
7	31	237	303	571
8	31	239	289	559
9	32	234	225	491
10	30	230	211	471
11	28	227	215	470
12	31	232	225	488
13	31	231	228	490
14	32	235	235	502
15	35	240	280	555
Average±SD	**30.8 ± 1.7**	**229.6 ± 7.0**	**260.2 ± 40.8**	**520.6 ± 39.9**

Absorbed dose values measured using radiochromic film were analyzed at points located on the applicator's surface and associated with the clinical target volume (CTV) and at points located 1-3 cm from the applicator (Table 3). The radiochromic film measurements in the printed model associated with representative points of the CTV generated deviations of 1.4% (1%-2%) in the locally absorbed dose, while the points 1-3 cm from the applicator exhibited a difference of 2.6%-6.2%.

Table 3:Difference in absorbed dose calculated by TPS vs absorbed dose measured with radiochromic film (RFD) in a 3D-printed model for points located 1-3 cm from the applicator. Diff: difference in percentage. SD: standard deviation.

Clinical Dose Points: Diff % Local Absorbed Dose

Distance from target	**Target**			**1 cm**			**2 cm**			**3 cm**		
Patients	**TPS**	**RFD**	**Diff (%)**	**TPS**	**RFD**	**Diff (%)**	**TPS**	**RFD**	**Diff (%)**	**TPS**	**RFD**	**Diff (%)**

1	20	19.8	1.0%	8.5	8	5.9%	4	3.9	2.5%	2.4	2.2	8.3%
2	20.1	19.9	1.0%	8.2	7.9	3.7%	3.9	3.7	5.1%	2.5	2.4	4.0%
3	20	19.8	1.0%	8.4	8.2	2.4%	4	3.8	5.0%	2.5	2.35	6.0%
4	20	19.7	1.5%	8.3	8.1	2.4%	4.1	4	2.4%	2.7	2.5	7.4%
5	20.2	19.8	2.0%	8.1	8	1.2%	4	3.8	5.0%	2.4	2.4	0.0%
6	19.9	19.6	1.5%	7.8	7.5	3.8%	4.2	3.9	7.1%	2.3	2.2	4.3%
7	20	19.6	2.0%	7.9	7.7	2.5%	4.1	4	2.4%	2.5	2.4	4.0%
8	20	19.6	2.0%	8.2	8.1	1.2%	4.2	4	4.8%	2.6	2.3	11.5%
9	20.1	19.8	1.5%	8.1	8	1.2%	3.8	3.7	2.6%	2.6	2.4	7.7%
10	19.9	19.5	2.0%	8	7.7	3.8%	4.1	4	2.4%	2.7	2.5	7.4%
11	20	19.9	0.5%	8.1	7.8	3.7%	4	3.9	2.5%	2.8	2.5	10.7%
12	20	19.8	1.0%	8.1	7.9	2.5%	4.2	4	4.8%	2.5	2.4	4.0%
13	20.4	20.2	1.0%	8	7.9	1.3%	4.1	3.8	7.3%	2.5	2.4	4.0%
14	20.3	20	1.5%	8.1	8	1.2%	4	3.9	2.5%	2.4	2.3	4.2%
15	19.8	19.5	1.5%	8.2	8	2.4%	3.8	3.7	2.6%	2.3	2.1	8.7%
Average±SD	20.0±0.2	19.8±0.2	1.4%	8.1±0.2	7.9±0.2	2.6%	4.0±0.1	3.9±0.1	3.9%	2.5±0.1	2.4±0.1	6.2%

DISCUSSION

The significant advancements in image-based recording and therapy planning have greatly improved radiotherapy over the past 40 years. However, these developments have had little impact on IORT [5]. In contrast, External Beam Radiotherapy has benefited from the development of increasingly sophisticated TPS with more powerful calculation algorithms and the ability to work with image sets. The lack of progress in IORT planning systems can be attributed to the challenges of installing useful in-room imaging in the OR in the past. Modern treatment planning requires 3D imaging, which interferes with the limited space in the OR, prolongs operation time, and is difficult to position without disrupting the sterile surgical environment.

One of the main existing planning system for IORT [38], which combines surgical navigation with elaborate tools for volume rendering of CT images. This system offers the possibility of simulating a surgical cavity, defining an applicator's position and angle, and calculating the dose distribution. The system employs different calculation algorithms that are increasingly faster and more reliable [39]. This system can be used to pre-plan the surgical IORT procedure or reconstruct the dose distribution through an independent CT study.

The optimal approach for computing absorbed dose involves using CT imaging, but this may not always be available in situations where intraoperative CT equipment is unavailable. However, real-time images of the area to be irradiated can be obtained using photogrammetry at the moment of treatment delivery, without the need for CT images or extra equipment. This approach can be applied in any OR using only a smartphone or tablet for imaging.

In this study, the time required to obtain adequate video images is only 30.8 seconds. From these images, the system takes 229.6 seconds to generate the 3D object where the absorbed dose is calculated in just 0.01 seconds. Real-time performance rates depend on the eventual application [40–42] . After adding the time for photogrammetry-based image acquisition, 3D reconstruction, and planning and evaluation, the entire process took less than 10 minutes in all cases analyzed for this surgery planning tool.

Planning and evaluation can be carried out in parallel with other actions aimed at preparing the tumor bed for irradiation, minimizing the loss of time in the OR. This technique enables the calculation of the absorbed dose in the tumor bed and allows for real-time decisions to be made regarding dose prescription and applicator placement, optimizing treatment.

The aim of this study was to commission a TPS using radiochromic film measurements in a 3D-printed model. The objective was to evaluate the accuracy of the TPS by determining whether the calculated dose in clinically significant areas yielded satisfactory results. The radiochromic films were calibrated to simulate the beam hardening conditions of clinical practice. Each film was irradiated and calibrated using its corresponding calibration curve adjusted for beam hardening, resulting in improved accuracy of the results. The Multigaussian method was utilized for calibration [29], which optimized each channel in the corresponding dose range. Avanzo et al. [26] positioned the films 1-2 cm from the applicator, and the highest absorbed dose was 4.7 Gy, with an average of 2.22 Gy in the closest area. This value was comparable to the average absorbed dose in the skin obtained by Fogg et al [43]. Similarly, Ciocca et al [44] reported a mean deviation of 1.8% ± 4.7% between the expected dose and the *in vivo* measurement with radiochromic films.

In the context of low-energy sources, the photoelectric process prevails. Differences in mass-energy absorption coefficients among various tissues and water could result in significant dose variations depending on the medium chosen for radiation transport and energy deposition [45]. Taylor has demonstrated that the dose to local medium can differ from the dose to water by up to 25% for breast tissue, using the Xoft electronic miniature X-ray source, with the dose ratio changing by almost 25% over 5 cm [46].

The TG-43 parameters of a brachytherapy source were obtained in a homogeneous water phantom. However, in clinical practice, the brachytherapy sources are placed inside the patient's tissues, where the different mass absorption coefficients, radiation scattering, and attenuations in materials with different compositions could alter the dose distribution compared to water. There are also other tissues inside the human body, such as bone, breast, and lung, with more variations in density, atomic number, and chemical composition, for which TG-43 parameters show greater discrepancies than in the water phantom [47].

Duque et al. [48] reported on the dosimetric impact of replacing the TG-43 formalism with a model-based dose calculation for liver brachytherapy and found that the dose calculated with TG-186 [49] was, on average, lower than that calculated with TG-43. White et al [50] compared TG-43 and TG-186 in breast irradiation using Axxent® and reported that all simulated heterogeneous models yielded a dose that was smaller than the dose-volume-histogram metrics.

The measurements obtained using radiochromic film in the target (as shown in Table 3) exhibited differences of 1.4% as compared to the values calculated using the TPS. A notable limitation of the study is the absence of reconstruction of the tumor bed subsequent to applicator placement. The reconstructions were carried out prior to applicator placement to ensure proper reconstruction of the tumor bed and development of a 3D-printed model for measuring absorbed dose using radiographic films. However, reconstructions conducted with the applicator in place would solely reconstruct the surface of the applicator and not the tumor bed. In the current version, images are also captured with the applicator in place and merged with those of the tumor bed to enable more precise reconstruction of the surgical scenario. Nonetheless, this enhancement is still undergoing testing, the number of patients is limited, and the procedure is not yet fully validated.

Another limitation of the study is the density of the material used, as it does not match the density of the tissue, and it is impossible to create a 3D-printed model with the different density inhomogeneities in the tumor bed. In future versions of the computational model, it will be feasible to produce regions with different densities for the implementation of a computational model with correction for tissue heterogeneity.

In this procedure, OARs are not contoured. Instead, absorbed doses are estimated by measuring them at various distances from the applicator. For values measured between 1 cm and 3 cm (Table 3), a discrepancy range of 2.6% to 6.2% in locally absorbed dose was observed. This can be attributed to the rapid decay with distance at the low energies used, which leads to known differences in the TG-43 calculation formalism as we move away from the source [47]. Furthermore, even with careful selection of areas to place the radiochromic films, there is inherent uncertainty in this process. This explains the increasing differences between the calculated and measured absorbed dose as we move away from the target and is a limitation of the study.

The isodose curves in the tumor bed images enable modification of the treatment prescription, dwell times inside the applicator, and virtual applicator positioning to optimize treatment. The next objective of the TPS development is to implement a more precise calculation and to use pre-plan images in conjunction with surface images of the tumor bed obtained.

CONCLUSION

We introduced and validated the initial photogrammetry-based system for low-energy photon IORT planning, which has the capacity to capture real-time images within the OR immediately following tumor resection and prior to irradiation. The images are captured using a smartphone or tablet and processed using open-source software within the same application. Commissioning of the system was accomplished by producing 3D printed tumor beds and confirming absorbed doses at distinct points through precise calibration of radiochromic films with appropriate beam hardening. The commissioning was successful.

REFERENCES

[1] von Mehren M, Randall RL, Benjamin RS, Boles S, Bui MM, Ganjoo KN, et al. Soft Tissue Sarcoma, Version 2.2018, NCCN Clinical Practice Guidelines in Oncology. J Natl Compr Canc Netw 2018;16:536–63. https://doi.org/10.6004/jnccn.2018.0025.

[2] Roeder F, Krempien R. Intraoperative radiation therapy (IORT) in soft-tissue sarcoma. Radiat Oncol 2017;12:20. https://doi.org/10.1186/s13014-016-0751-2.

[3] Yang JC, Chang AE, Baker AR, Sindelar WF, Danforth DN, Topalian SL, et al. Randomized prospective study of the benefit of adjuvant radiation therapy in the treatment of soft tissue sarcomas of the extremity. J Clin Oncol Off J Am Soc Clin Oncol 1998;16:197–203. https://doi.org/10.1200/JCO.1998.16.1.197.

[4] Roeder F, Morillo V, Saleh-Ebrahimi L, Calvo FA, Poortmans P, Ferrer Albiach C. Intraoperative radiation therapy (IORT) for soft tissue sarcoma - ESTRO IORT Task Force/ACROP recommendations. Radiother Oncol J Eur Soc Ther Radiol Oncol 2020;150:293–302. https://doi.org/10.1016/j.radonc.2020.07.019.

[5] Hensley FW. Present state and issues in IORT Physics. Radiat Oncol 2017;12:37. https://doi.org/10.1186/s13014-016-0754-z.

[6] Supanich M, Siewerdsen J, Fahrig R, Farahani K, Gang GJ, Helm P, et al. AAPM Task Group Report 238: 3D C-arms with volumetric imaging capability*. Med Phys 2023;n/a. https://doi.org/https://doi.org/10.1002/mp.16245.

[7] Hassinger TE, Showalter TN, Schroen AT, Brenin DR, Berger AC, Libby B, et al. Utility of CT imaging in a novel form of high-dose-rate intraoperative breast radiation therapy. J Med Imaging Radiat Oncol 2018;62:835–40. https://doi.org/10.1111/1754-9485.12790.

[8] García-Vázquez V, Calvo FA, Ledesma-Carbayo MJ, Sole C V, Calvo-Haro J, Desco M, et al. Intraoperative computed tomography imaging for dose calculation in intraoperative electron radiation therapy: Initial clinical observations. PLoS One 2020;15:e0227155.

[9] Garcia-Gil R, Casans S, Edith Navarro A, García-Sánchez A-J, Rovira-Escutia JJ, Garcia-Costa D, et al. Embedded bleeding detector into a PMMA applicator for electron intraoperative radiotherapy. Phys Medica Eur J Med Phys 2022;94:35–42. https://doi.org/10.1016/j.ejmp.2021.12.018.

[10] Hartley R, Zisserman A. Multiple View Geometry in Computer Vision. 2nd ed. Cambridge: Cambridge University Press; 2004. https://doi.org/DOI: 10.1017/CBO9780511811685.

[11] Reljić I, Dunđer I, Seljan S. Photogrammetric 3D Scanning of Physical Objects: Tools and Workflow 2019;8:383–8. https://doi.org/10.18421/TEM82-09.

[12] Nath R, Anderson LL, Luxton G, Weaver KA, Williamson JF, Meigooni AS. Dosimetry of interstitial brachytherapy sources: recommendations of the AAPM Radiation Therapy Committee Task Group No. 43. American Association of Physicists in Medicine. Med Phys 1995;22:209–34.

https://doi.org/10.1118/1.597458.

[13] Rivard MJ, Davis SD, DeWerd LA, Rusch TW, Axelrod S. Calculated and measured brachytherapy dosimetry parameters in water for the Xoft Axxent X-Ray Source: an electronic brachytherapy source. Med Phys 2006;33:4020–32. https://doi.org/10.1118/1.2357021.

[14] Dickler A, Dowlatshahi K. Xoft Axxent electronic brachytherapy™. Expert Rev Med Devices 2009;6:27–31. https://doi.org/10.1586/17434440.6.1.27.

[15] AliceVision. Meshroom: A 3D reconstruction software (accesed 11/27/2020) 2018.

[16] Bouguet J-Y. Camera calibration toolbox for matlab, 2001.

[17] Wang J, Shi F, Zhang J, Liu Y. A new calibration model of camera lens distortion. Pattern Recognit 2008;41:607–15. https://doi.org/https://doi.org/10.1016/j.patcog.2007.06.012.

[18] Baldini EH, Abrams RA, Bosch W, Roberge D, Haas RLM, Catton CN, et al. Retroperitoneal Sarcoma Target Volume and Organ at Risk Contour Delineation Agreement Among NRG Sarcoma Radiation Oncologists. Int J Radiat Oncol Biol Phys 2015;92:1053–9. https://doi.org/10.1016/j.ijrobp.2015.04.039.

[19] Vries J de. LearnOpenGL (accesed 05-04-2021) 2014. www.learnopengl.com (accessed May 4, 2021).

[20] Bevilacqua F. CVUI: A (very) simple library on top of OpenCV (accesed 06-24-2021) 2016.

[21] Hill R, Kuncic Z, Baldock C. The water equivalence of solid phantoms for low energy photon beams. Med Phys 2010;37:4355–63. https://doi.org/10.1118/1.3462558.

[22] Installation and Usage Instructions Form 3 Low Force Stereolithography (LFS) 3D Printer n.d. https://media.formlabs.com/m/5a3f3cadc639b857/original/-ENUS-Form-3-Manual.pdf (accessed May 5, 2022).

[23] Elastic A50 (formlabs) n.d. https://formlabs.com/blog/elastic-resin-soft-resilient-3d-printing/.

[24] Severgnini M, de Denaro M, Bortul M, Vidali C, Beorchia A. In vivo dosimetry and shielding disk alignment verification by EBT3 GAFCHROMIC film in breast IOERT treatment. J Appl Clin Med Phys 2014;16:5065. https://doi.org/10.1120/jacmp.v16i1.5065.

[25] Petoukhova A, Rüssel I, Nijst-Brouwers J, van Wingerden K, van Egmond J, Jacobs D, et al. In vivo dosimetry with MOSFETs and GAFCHROMIC films during electron IORT for Accelerated Partial Breast Irradiation. Phys Medica 2017;44:26–33. https://doi.org/10.1016/j.ejmp.2017.11.004.

[26] Avanzo M, Rink A, Dassie A, Massarut S, Roncadin M, Borsatti E, et al. In vivo dosimetry with radiochromic films in low-voltage intraoperative radiotherapy of the breast. Med Phys 2012;39:2359–68. https://doi.org/10.1118/1.3700175.

[27] Devic S, Tomic N, Lewis D. Reference radiochromic film dosimetry: Review of technical aspects. Phys Medica 2016;32:541–56. https://doi.org/https://doi.org/10.1016/j.ejmp.2016.02.008.

[28] McCabe BP, Speidel MA, Pike TL, Van Lysel MS. Calibration of GafChromic XR-RV3 radiochromic film for skin dose measurement using standardized x-ray spectra and a commercial flatbed scanner. Med Phys 2011;38:1919–30. https://doi.org/10.1118/1.3560422.

[29] Méndez I, Polšak A, Hudej R, Casar B. The Multigaussian method: a new approach to mitigating spatial heterogeneities with multichannel radiochromic film dosimetry. Phys Med Biol 2018;63:175013. https://doi.org/10.1088/1361-6560/aad9c1.

[30] Lozares S, Font JA, Gandía A, Campos A, Flamarique S, Ibáñez R, et al. In vivo dosimetry in low-voltage IORT breast treatments with XR-RV3 radiochromic film. Phys Medica 2021;81:173–81. https://doi.org/https://doi.org/10.1016/j.ejmp.2020.12.011.

[31] Farah J, Trianni A, Ciraj-Bjelac O, Clairand I, De Angelis C, Delle Canne S, et al. Characterization of XR-RV3 GafChromic® films in standard laboratory and in clinical conditions and means to evaluate uncertainties and reduce errors. Med Phys 2015;42:4211–26. https://doi.org/10.1118/1.4922132.

[32] Richter C, Pawelke J, Karsch L, Woithe J. Energy dependence of EBT-1 radiochromic film response for photon and electron beams readout by a flatbed scanner. Med Phys 2009;36:5506–14. https://doi.org/10.1118/1.3253902.

[33] Vera-Sánchez JA, Ruiz-Morales C, González-López A. Monte Carlo uncertainty analysis of dose estimates in radiochromic film dosimetry with single-channel and multichannel algorithms. Phys Medica 2018;47:23–33. https://doi.org/10.1016/j.ejmp.2018.02.006.

[34] Ma CM, Coffey CW, DeWerd LA, Liu C, Nath R, Seltzer SM, et al. AAPM protocol for 40-300 kV x-ray beam dosimetry in radiotherapy and radiobiology. Med Phys 2001;28:868–93. https://doi.org/10.1118/1.1374247.

[35] IAEA TRS 398. Absorbed Dose Determination in External Beam Radiotherapy. Vienna: INTERNATIONAL ATOMIC ENERGY AGENCY; 2001. https://doi.org/10.1097/00004032-200111000-00017.

[36] Devic S, Seuntjens J, Sham E, Podgorsak EB, Schmidtlein CR, Kirov AS, et al. Precise radiochromic film dosimetry using a flat-bed document scanner. Med Phys 2005;32:2245–53. https://doi.org/10.1118/1.1929253.

[37] Devic S, Tomic N, Soares CG, Podgorsak EB. Optimizing the dynamic range extension of a radiochromic film dosimetry system. Med Phys 2009;36:429–37. https://doi.org/10.1118/1.3049597.

[38] Valdivieso-Casique MF, Rodríguez R, Rodríguez-Bescós S, Lardíes D, Guerra P, Ledesma MJ, et al. RADIANCE—A planning software for intra-operative radiation therapy. Transl Cancer Res Vol 4, No 2 (April 2015) Transl Cancer Res

(Intraoperative Radiother II) 2015.

[39] Tavallaie M, Hariri Tabrizi S, Heidarloo N. Implementation of pencil beam redefinition algorithm (PBRA) for intraoperative electron radiation therapy (IOERT) treatment planning. Phys Medica Eur J Med Phys 2022;104:32–42. https://doi.org/10.1016/j.ejmp.2022.10.015.

[40] González D, Cueto E, Chinesta F. Computational Patient Avatars for Surgery Planning. Ann Biomed Eng 2016;44:35–45. https://doi.org/10.1007/s10439-015-1362-z.

[41] Quesada C, Alfaro I, González D, Chinesta F, Cueto E. Haptic simulation of tissue tearing during surgery. Int j Numer Method Biomed Eng 2018;34:e2926. https://doi.org/https://doi.org/10.1002/cnm.2926.

[42] Badías A, González D, Alfaro I, Chinesta F, Cueto E. Real-time interaction of virtual and physical objects in mixed reality applications. Int J Numer Methods Eng 2020;121:3849–68. https://doi.org/https://doi.org/10.1002/nme.6385.

[43] Fogg P, Das KR, Kron T, Fox C, Chua B, Hagekyriakou J. Thermoluminescence dosimetry for skin dose assessment during intraoperative radiotherapy for early breast cancer. Australas Phys Eng Sci Med 2010;33:211–4. https://doi.org/10.1007/s13246-010-0019-3.

[44] Ciocca M, Orecchia R, Garibaldi C, Rondi E, Luini A, Gatti G, et al. In vivo dosimetry using radiochromic films during intraoperative electron beam radiation therapy in early-stage breast cancer. Radiother Oncol 2003;69:285–9. https://doi.org/https://doi.org/10.1016/j.radonc.2003.09.001.

[45] White DR, Booz J, Griffith R V, Spokas JJ, Wilson IJ. Report 44. J Int Comm Radiat Units Meas 1989;os23:NP-NP. https://doi.org/10.1093/jicru/os23.1.Report44.

[46] Taylor REP. “Monte Carlo Calculations for Brachytherapy” M. Sc. thesis. Carleton University, Ottawa (Canada), 2006.

[47] Zehtabian M, Faghihi R, Sina S. A Review on Main Defects of TG-43, 2012. https://doi.org/10.5772/34360.

[48] Duque AS, Corradini S, Kamp F, Seidensticker M, Streitparth F, Kurz C, et al. The dosimetric impact of replacing the TG-43 algorithm by model based dose calculation for liver brachytherapy. Radiat Oncol 2020;15:60. https://doi.org/10.1186/s13014-020-01492-9.

[49] Beaulieu L, Carlsson Tedgren Å, Carrier JF, Davis SD, Mourtada F, Rivard MJ, et al. Report of the Task Group 186 on model-based dose calculation methods in brachytherapy beyond the TG-43 formalism: Current status and recommendations for clinical implementation. Med Phys 2012;39:6208–36. https://doi.org/10.1118/1.4747264.

[50] White SA, Landry G, Fonseca GP, Holt R, Rusch T, Beaulieu L, et al. Comparison of TG-43 and TG-186 in breast irradiation using a low energy electronic brachytherapy source. Med Phys 2014;41. https://doi.org/10.1118/1.4873319.

FIGURE CAPTIONS

Figures:

Figure 1: Example of Meshroom reconstruction. From the extracted frames of the video (a), the software obtains the depth maps (b), which are used to create the final mesh (c).

Figure 2: System of coordinates used for TG-43 formalism [12].

Figure 3: PDD measured with radiochromic films and solid water phantom.

Figure 4: Measurement scheme with radiochromic film on the surface of the applicator in a mini-water tank.

Figure 5: System reconstructed model vs. 3D printed model for one of the cases.

Figure 6: (a) Absorbed doses calculated perpendicular plane to the applicator (b) Interface: dwell times, dwell positions, source parameters.

Figure 7: Selection of measurement points and placement of radiochromic films on the 3D model.

Figure 8: PDDs compared for the company's measurements with Exradin A50, those made with Tm-23342 and radiochromic films.

Figure 9: Calibration curves for radiochromic film with different applicators.

AUTHOR CONTRIBUTIONS STATEMENT

Each author has made substantial contributions to the conception or design of the work; or the acquisition, analysis, or interpretation of data; or the creation of new software used in the work; or have drafted the work or substantively revised it. Specifically, each work area was distributed as follows: Project design: SL, DG, AB, RI. State of the art: SL, AG, VG, JF; Patient selection: LL, RI, JP; Image acquisition: SL, RI, LL, JP, AG. Validation of images and selection of areas of interest. LL, RI, JP. Image processing and 3D reconstruction. CB, DG, AB. Calculation of dose distribution, methodology design and programming. CB, SL, DG, AB. Matlab Prototyping. CB, DG, AB. Implementation of the code in C++ and OpenGL: CB, DG, AB. Absorbed dose verification, 3D printing and calibration of radiochromic films: OB, SL, AG, VG, JF. Writing drafts of the article and subsequent detailed reviews: SL, VG. Each author has approved the submitted version.

DATA AVAILABILITY STATEMENT

The authors confirm that the data supporting the findings of this study are available within the article and its supplementary materials. The code is available in an open-source repository: http://github.com/cberbarbanoj/TG-43-Estimator

ADDITIONAL INFORMATION

Competing interests

The authors declare no competing interests.

Figure 1

Click here to access/download;Figure;Figure 1.jpg

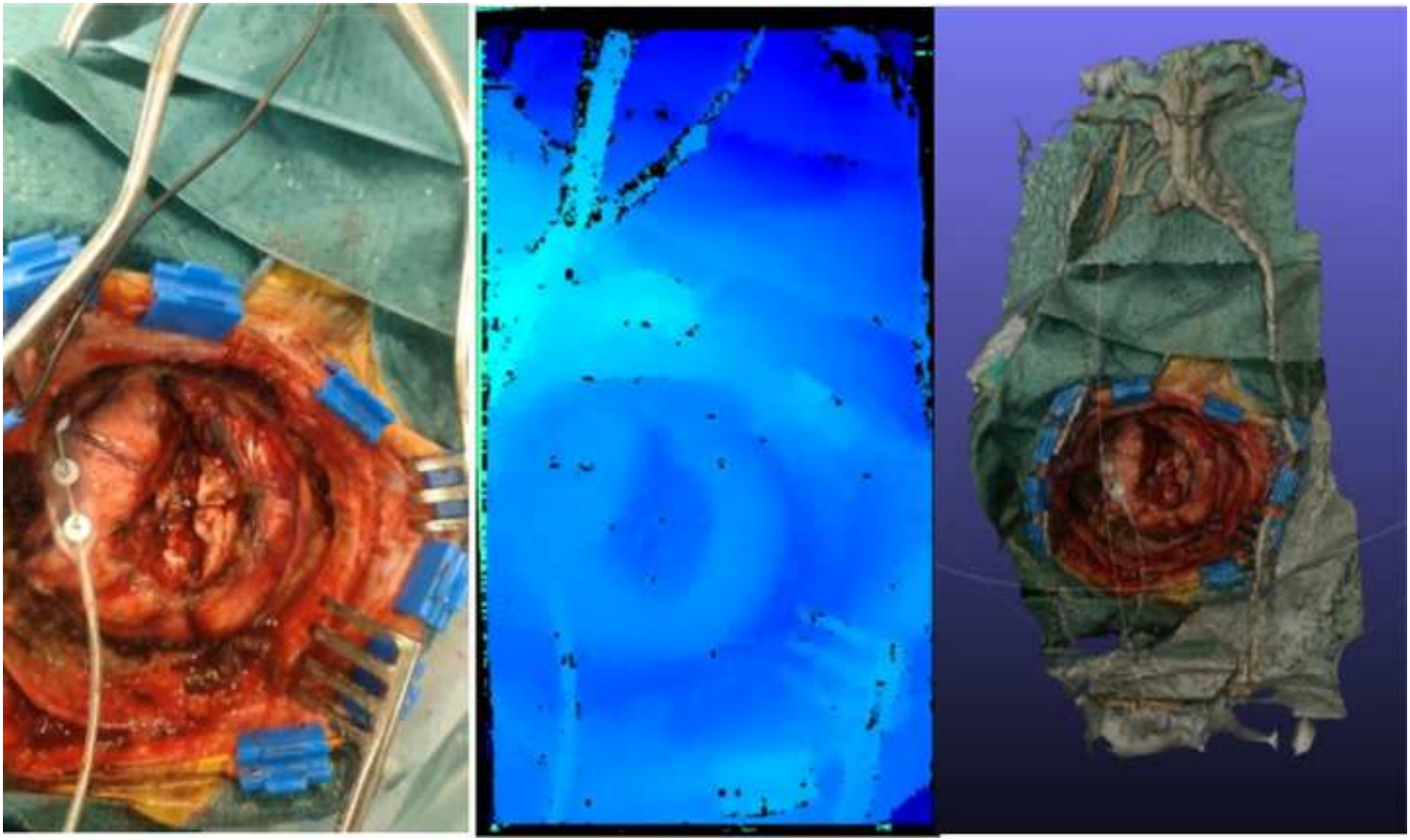

Figure 2

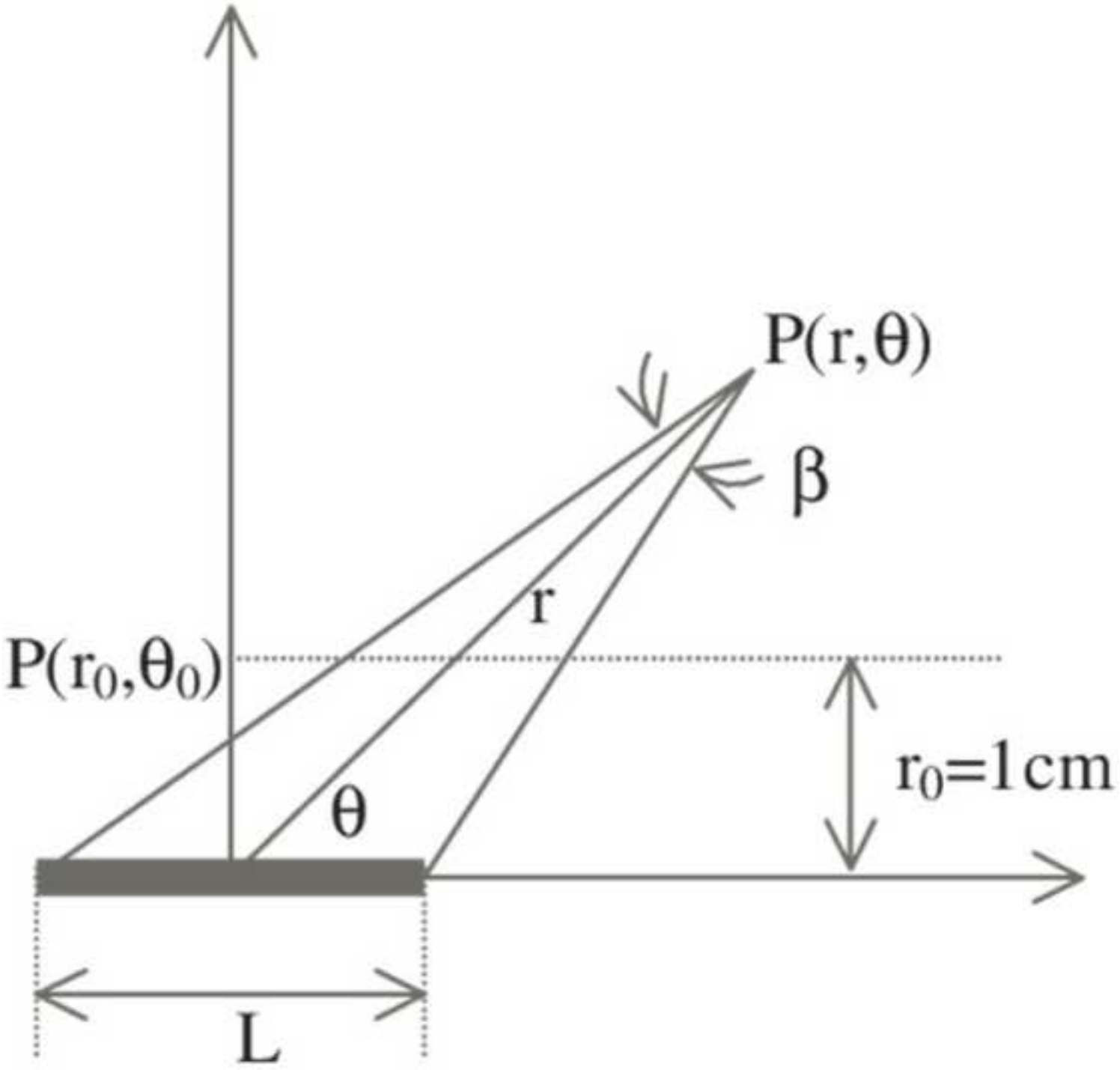

Figure 3

Click here to access/download;Figure;Figure 3.jpg

Figure 4

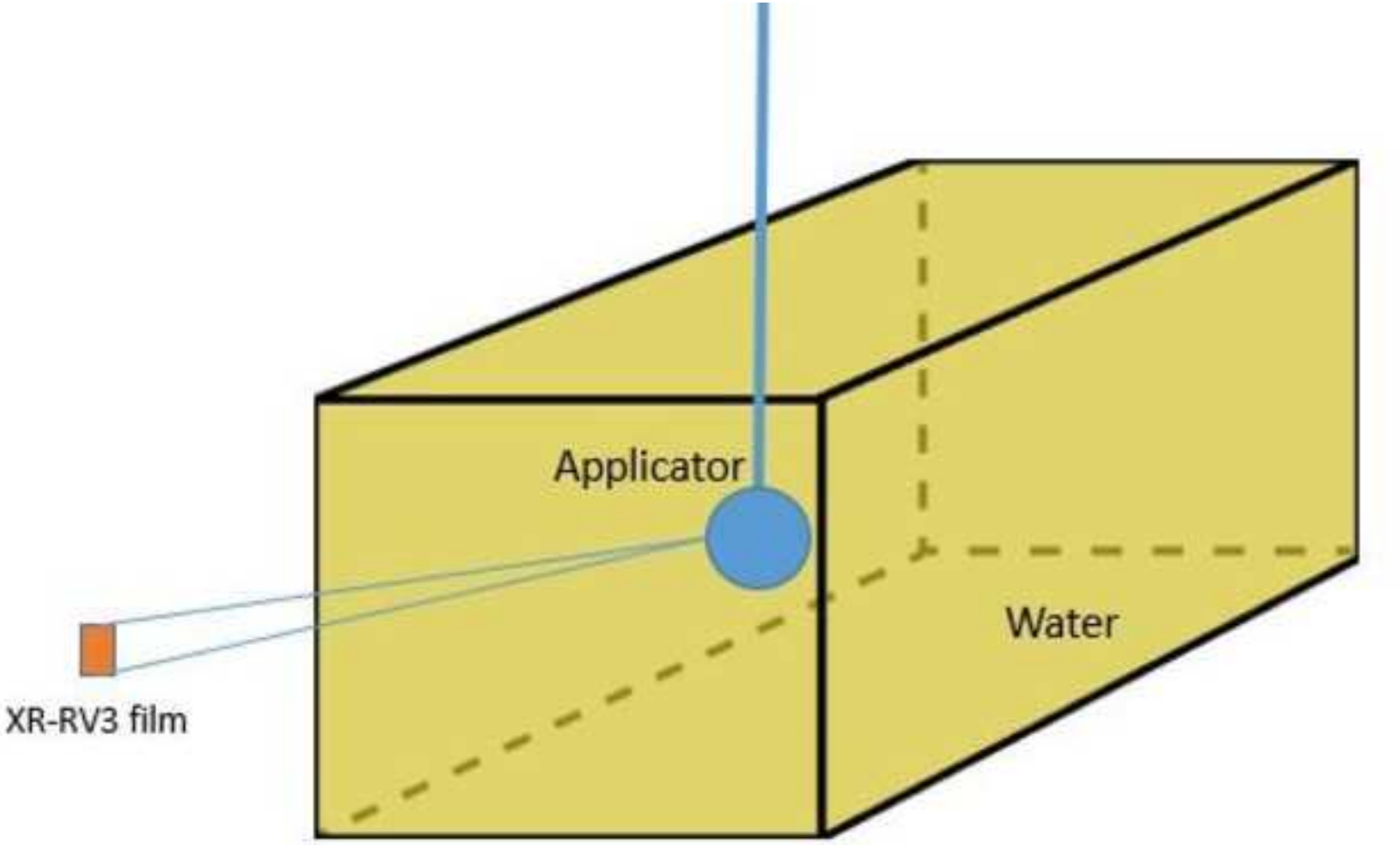

Figure 5

Click here to access/download;Figure;Figure 5.jpg

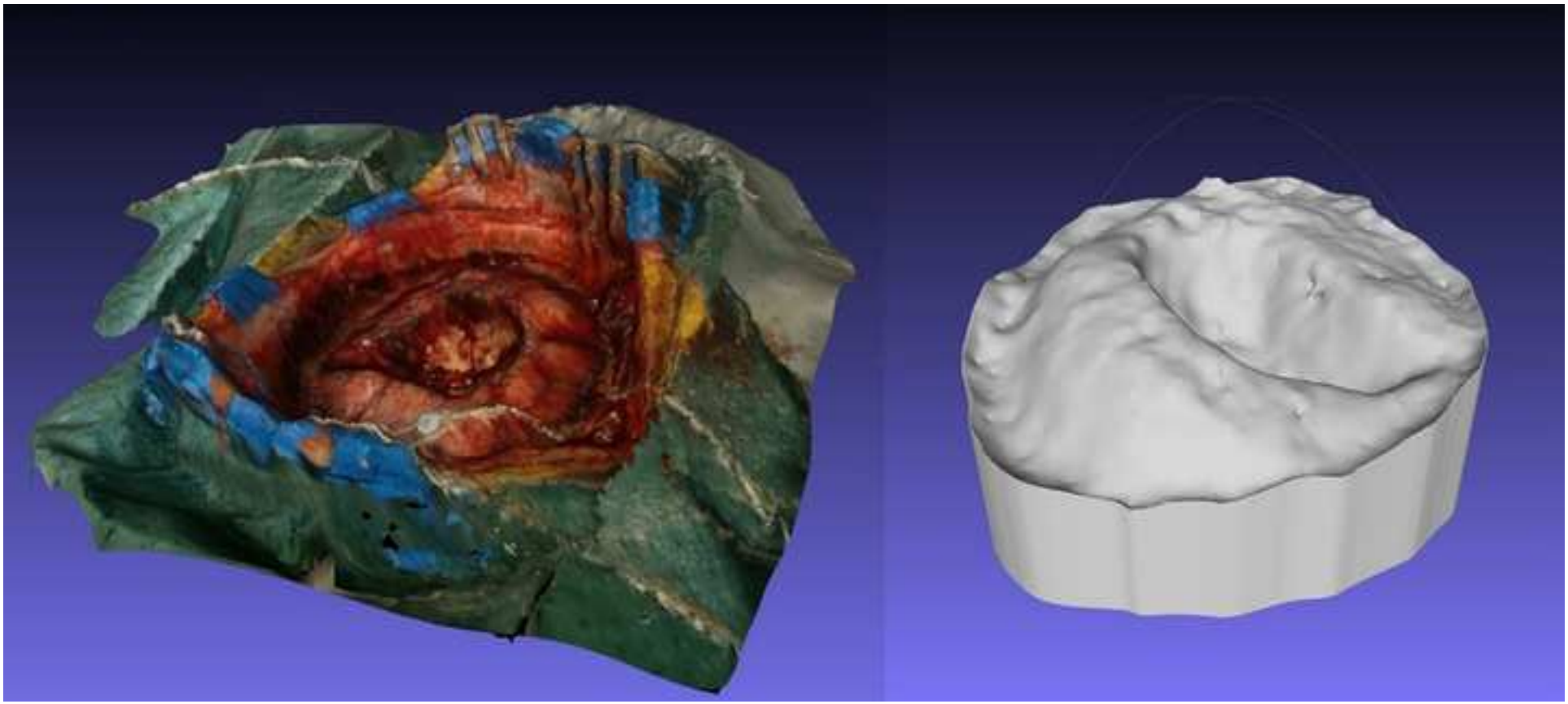

Figure 6a

Click here to access/download;Figure;Figure 6a.jpg

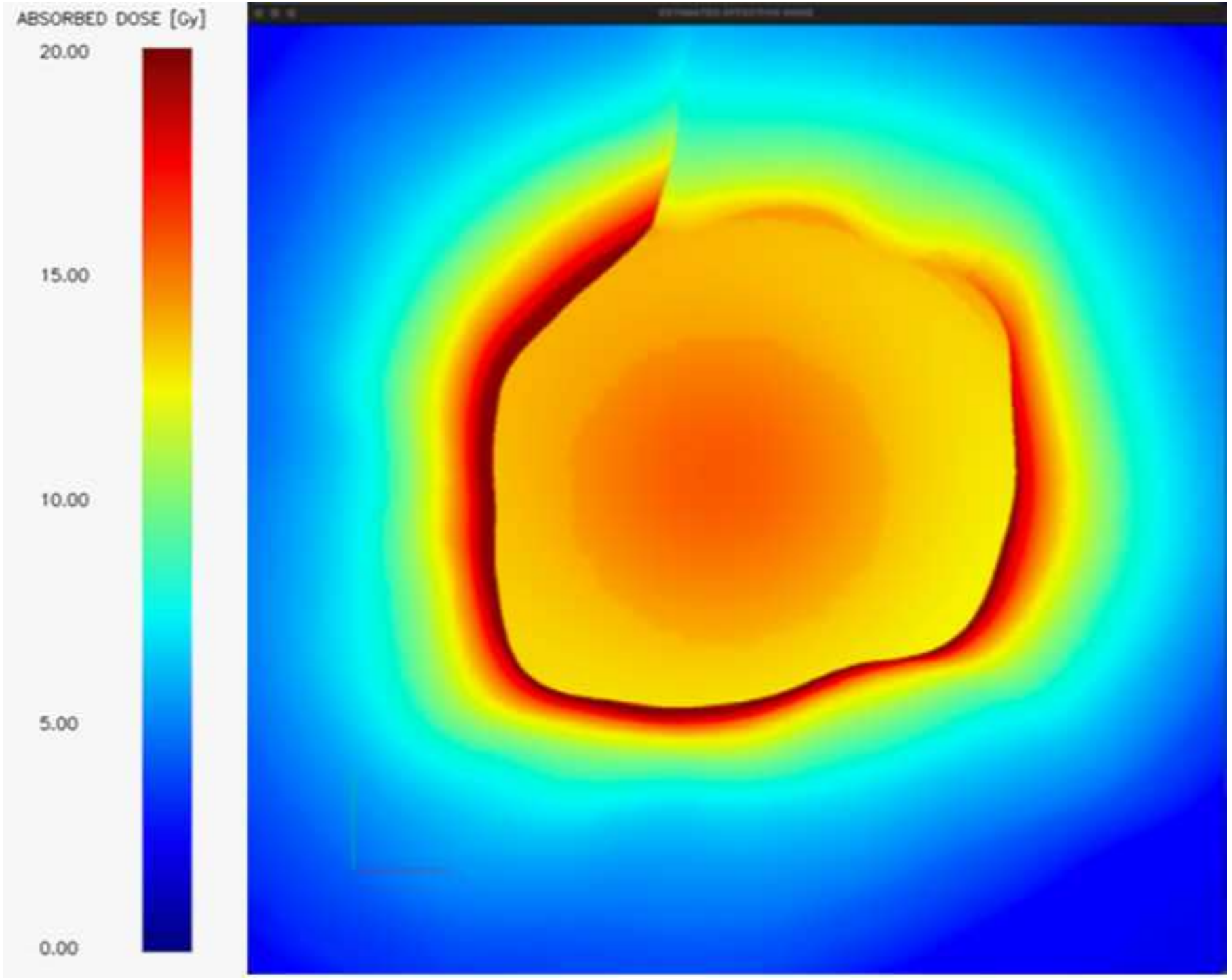

Figure 6b

Click here to access/download;Figure;Figure 6b.jpg

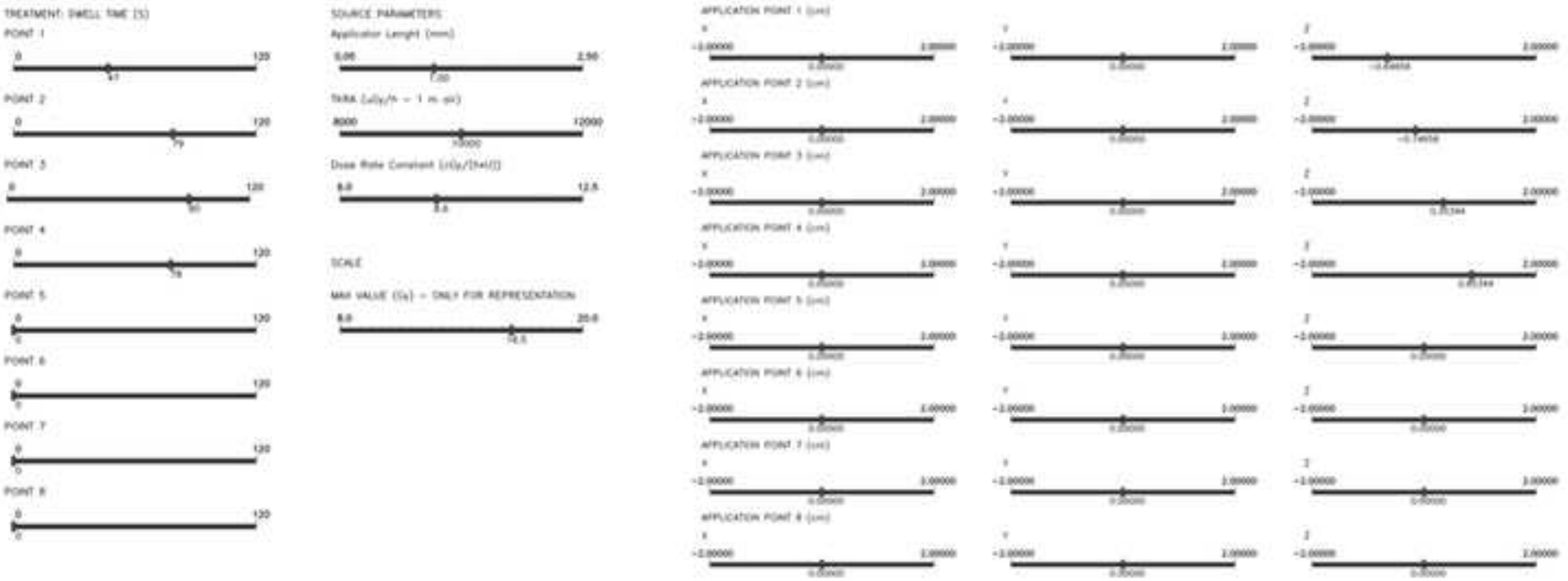

Figure 7

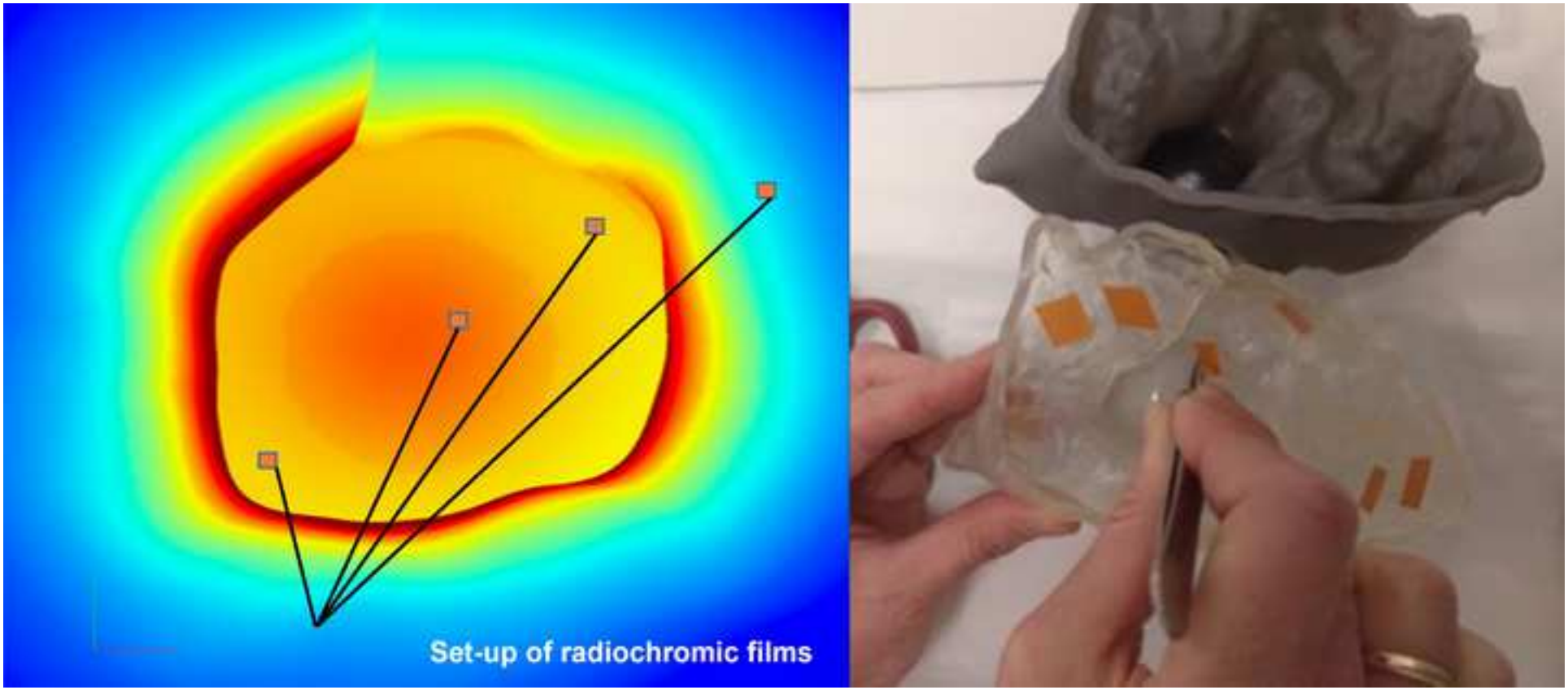

Figure 8

Click here to access/download;Figure;Figure 8.jpg

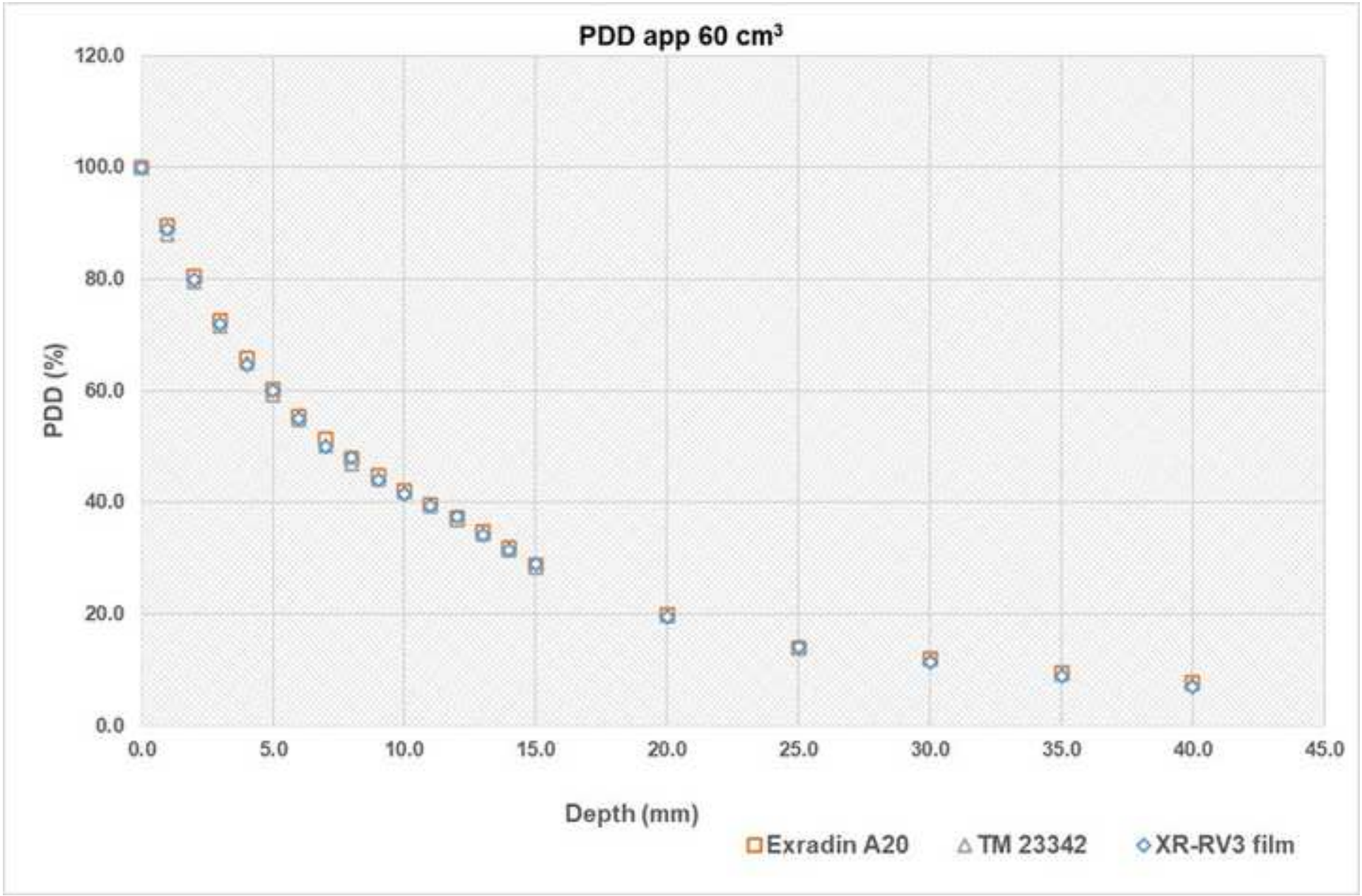

Figure 9

Click here to access/download;Figure;Figure 9.jpg